Journal of Sound and Vibration (1999) **219**(5), 785–812
Article No. jsvi.1998.1876, available online at http://www.idealibrary.com on IDEAL

DEVELOPMENT OF APPROXIMATE METHODS FOR THE ANALYSIS OF PATCH DAMPING DESIGN CONCEPTS

S.-W. KUNG AND R. SINGH

Acoustics and Dynamics Laboratory, *Department of Mechanical Engineering*, *The Ohio State University*, *Columbus*, *OH* 43210-1107, *U.S.A.*

(*Received* 15 *December* 1997, *and in final form* 8 *July* 1998)

This paper develops three approximate methods for the analysis of patch damping designs. Undamped natural frequencies and modal loss factors are calculated using the Rayleigh energy method and modal strain energy technique, respectively, without explicitly solving high order differential equations or complex eigenvalue problems. Approximate Method I is developed for sandwich beams assuming that damped mode shapes are given by the Euler beam eigenfunctions. The superposition principle is then used to accommodate any arbitrary mode shape, which may be obtained from modal experiments or the finite element method. In Method II, the formulation is further simplified with the assumption of a very compliant viscoelastic core. Finally, Method III considers a compact patch problem. The modal loss factor is then expressed as a product of terms related to material properties, layer thickness, patch size and patch performance. Approximate Methods II and III are also extended to rectangular plates. Formulations are verified by conducting analogous modal measurements and by comparing predictions with those obtained using the Rayleigh–Ritz method (without making any of the above mentioned assumptions). Several example cases are presented to demonstrate the validity and utility of approximate methods for patch damping design concepts.

1. INTRODUCTION

Patch damping design is an efficient and cost effective concept for solving noise and vibration problems [1–4]. However, there is a limited body of scientific literature on this topic and it therefore remains a somewhat ill-understood and empirical technique. Single or double constrained layer patches have been computationally examined by using higher order differential equation theory [3–7], the Rayleigh–Ritz method [1–4, 8, 9], or a finite element procedure [10–12]. Experimental methods of investigation have included modal testing [1–4] and structural intensity mapping [13]. The authors of this article have undertaken a comprehensive study of this topic and have proposed a new computational scheme, based on the Rayleigh–Ritz method, for beams and plates with multiple patches of arbitrary properties [1, 2]. Our calculation methods have been

0022–460X/99/050785 + 28 $30.00/0

verified by comparing results with measured modal data or those available in the literature.

The current paper extends prior work [1, 2] by proposing three approximate analytical methods. An attempt is being made to seek some insight into the patch damping design process. Tractable formulations that identify the role of the following parameters are developed: material properties, viscoelastic layer thickness, patch size, number of patches and their locations. Like the previous articles, cantilever beams and rectangular plates (with free–free or simply supported edges) serve as prime examples, and experimental modal analysis and the Rayleigh–Ritz method are used to examine the validity of each method. Key assumptions which form the basis of each method are: (1) the damped mode shapes of a sandwich beam may be described by the eigenfunctions of undamped Euler's beam [14], (2) the viscoelastic core layer is very compliant, and (3) only a single compact patch is applied. The last two assumptions are also applied to the plate example. Approximate methods are expected to be computationally efficient and suitable for rapid parametric design studies.

2. APPROXIMATE METHOD I FOR SANDWICH BEAMS

2.1. Euler beam modes

The structure of interest is an elastic beam (designated as layer 3) with N_p damping patches attached, as shown in Figure 1. Each patch p of length l_x^p is located at x^p, and has two layers: layer 1 is an elastic layer while layer 2 is made of viscoelastic material. Note that each patch may be different in size, thickness and material property. The analytical approach, to be developed in this section, is called Approximate Method I since one assumption is made in addition to those usually made for a sandwich beam [5]. Specifically, the kth damped mode shape

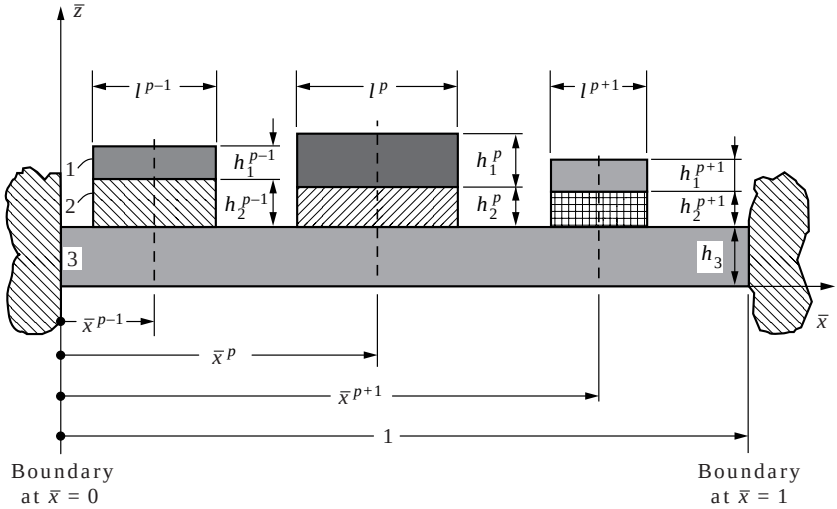

Figure 1. Beam with multiple constrained layer damping patches. Layer 1 = constraining layer (elastic), layer 2 = constrained layer (viscoelastic), layer 3 = base structure (elastic).

TABLE 1

Euler beam eigenfunction coefficients for selected boundary conditions

k	λ_k	a_k	b_k	c_k	d_k
A. Simply-supported beam					
1	3·1416	$\sqrt{2}$	0	0	0
2	6·2832	$\sqrt{2}$	0	0	0
3	9·4248	$\sqrt{2}$	0	0	0
4	12·5664	$\sqrt{2}$	0	0	0
⋮	⋮	⋮	⋮	⋮	⋮
n	$n\pi$	$\sqrt{2}$	0	0	0
B. Clamped–free beam					
1	1·8751	0·7341	−1	−0·7341	1
2	4·6941	1·0185	−1	−1·0185	1
3	7·8548	0·9992	−1	−0·9992	1
4	10·9955	1·0000	−1	−1·0000	1
⋮	⋮	⋮	⋮	⋮	⋮
n	$(2n-1)\pi/2$	1	−1	−1	1
C. Free–free beam					
1	4·7300	−0·9825	1	−0·9825	1
2	7·8532	−1·0008	1	−1·0008	1
3	10·9956	−1·0000	1	−1·0000	1
4	14·1372	−1·0000	1	−1·0000	1
⋮	⋮	⋮	⋮	⋮	⋮
n	$(2n+1)\pi/2$	−1	1	−1	1

of the sandwich beam is approximated by the eigenfunction (w_k) of an undamped Euler beam that is described as follows where λ_k is the frequency parameter of mode k and $\bar{x} = x/l_x$:

$$\frac{\mathrm{d}^4 w_k}{\mathrm{d}\bar{x}^4} = \lambda_k^4 w_k,$$

$$w_k(\bar{x}) = a_k \sin(\lambda_k \bar{x}) + b_k \cos(\lambda_k \bar{x}) + c_k \sinh(\lambda_k \bar{x}) + d_k \cosh(\lambda_k \bar{x}), \quad \text{(1a, b)}$$

where a_k, b_k, c_k and d_k, are coefficients whose sample values for selected boundary conditions are listed in Table 1, for the sake of completeness. Refer to reference [15] for other cases.

Taking advantage of equation (1), the corresponding longitudinal (u_k) and shear deformation (γ_k) mode shapes will be derived in the next section. The Rayleigh method along with modal strain energy technique are then used to explicitly obtain the undamped natural frequency (ω_k) and modal loss factor (η_k) without solving for a complex eigenvalue problem.

2.2. KINEMATIC RELATIONSHIPS

Other deformation variables are longitudinal shapes $u_{1,k}^p$ and $u_{3,k}$ of layers 1 and 3, and shear deformation shape $\gamma_{2,k}^p$ of layer 2 for $p = 1 \cdots N_p$. To express these

in terms of the flexural shape w_k, some kinematic relationships must be used. First, the relationship between $u^p_{1,k}$ and $u_{3,k}$ can be written by extending the integrated form of the weak core assumption [1]:

$$u^p_{3,k} = -e^p u_{1,k} + s^p_k, \tag{2}$$

where

$$e^p = \frac{E^p_1 h^p_1}{E_3 h_3}; \quad p = 1, \ldots, N_p. \tag{3}$$

Note that s^p_k is the constant that relates deformation shape $u^p_{1,k}$ to the corresponding $u_{3,k}$ for each patch p. Second, by observing Figure 2, the relationship between the shear deformation shape $\gamma^p_{2,k}$ and longitudinal displacements $u^p_{1,k}$ and $u_{3,k}$ is

$$\gamma^p_{2,k} = \frac{1}{h_2}\left(u^p_{1,k} - u_{3,k} + \frac{C^p}{l_x}\frac{\mathrm{d}w_k}{\mathrm{d}\bar{x}}\right), \tag{4}$$

where $C^p = (h^p_1 + 2h^p_2 + h_3)/2$ (see Appendix B for detailed derivations). Also, from equations (2) and (4), $\gamma^p_{2,k}$ can be expressed as

$$\gamma^p_{2,k} = \frac{1}{h_2}\left((1 + e^p)u_{1,k} + \frac{C^p}{l_x}\frac{\mathrm{d}w_k}{\mathrm{d}\bar{x}} - s^p_k\right). \tag{5}$$

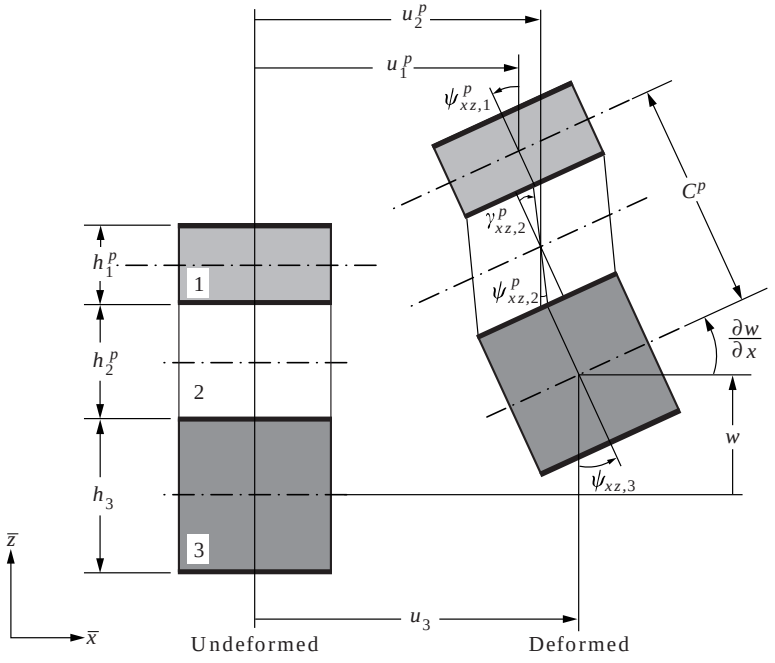

Figure 2. Undeformed and deformed segments, with variables in all layers. Key as for Figure 1.

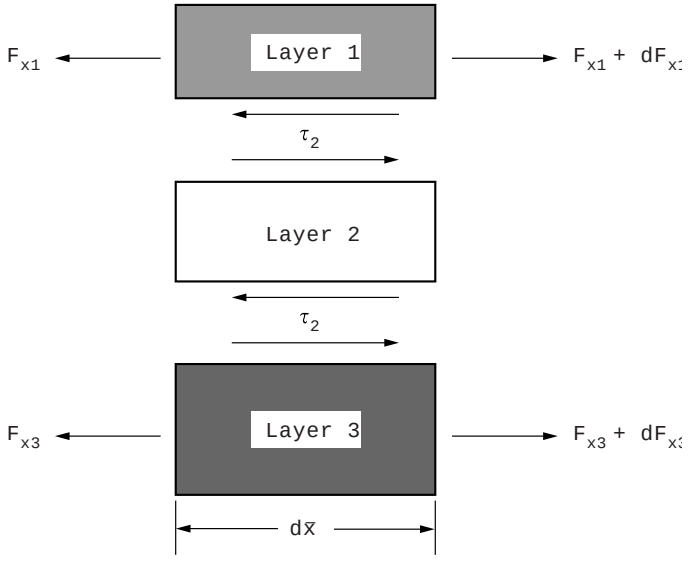

Figure 3. Axial force and shear stress relationships for a segment of the sandwich beam. Key as for Figure 1.

Finally, consider the free body diagram of a beam section of length $d\bar{x}$ as illustrated in Figure 3. Relationships between the axial force $F_{x1,k}$, longitudinal displacement $u^p_{1,k}$, and the shear stress $\tau^p_{2,k}$ and strain $\gamma^p_{2,k}$ are

$$\tau^p_{2,k} l_x \, d\bar{x} = dF_{x1,k}; \qquad F_{x1,k} = E^p_1 h^p_1 \frac{du^p_{1,k}}{l \, d\bar{x}}; \qquad \tau^p_{2,k} = G_2 \gamma^p_{2,k}. \tag{6a–c}$$

Combining equations (5) and (6), a differential equation in terms of $u_{3,k}$ is found to be

$$\frac{d^2 u^p_{1,k}}{d\bar{x}^2} = \frac{G^p_2 I^2_x}{E^p_1 h^p_1 h^p_2} \left[(e^p + 1) u^p_{1,k} + \frac{C^p}{l_x} \frac{dw_k}{d\bar{x}} - s^p_k \right]. \tag{7}$$

Corresponding shapes are derived in the next two sections using equations (5) and (7).

2.3. CORRESPONDING LONGITUDINAL SHAPES

To solve the second order differential equation (7) in terms of $u^p_{1,k}$, ignore constant s^p_k for the sake of simplification. This assumption is reasonable since it does not affect the longitudinal strain energy. Equation (7) is rewritten as

$$\frac{d^2 u^p_{1,k}}{d\bar{x}^2} - Y^p u^p_{1,k} = \frac{Y^p C^p}{l_x (e^p + 1)} \frac{dw_k}{d\bar{x}}, \qquad Y^p = G^p_2 I^2_x (e^p + 1) / E^p_1 h^p_1 h^p_2. \tag{8a, b}$$

Taking advantage of equation (1), the solution to equation (8) is obtained as

$$u^p_{1,k}(\bar{x}) = A^p_k \sinh(\sqrt{Y^p}\bar{x}) + B^p_k \cosh(\sqrt{Y^p}\bar{x}) + \mu^p_k Y^p \frac{dw_k}{\partial \bar{x}} + \mu^p_k \frac{d^3 w_k}{d\bar{x}^3}, \tag{9}$$

where

$$\mu_k^p = \frac{C^p Y^p}{l_x(e^p+1)[\lambda_k^4 - (Y^p)^2]}. \tag{10a, b}$$

Constants A_k^p and B_k^p of equation (9) must be determined in accordance with the longitudinal boundary conditions of layer 1. For a damping patch with free ends at $\bar{x}_a^p = \bar{x}^p - 0{\cdot}5\bar{l}_x^p$ and $\bar{x}_b^p = \bar{x}^p + 0{\cdot}5\bar{l}_x^p$, A_k^p and B_k^p can be calculated as follows by applying boundary conditions $\mathrm{d}u_3(\bar{x}_a^p)/\mathrm{d}\bar{x} = 0$ and $\mathrm{d}u_3(\bar{x}_b^p)/\mathrm{d}\bar{x} = 0$ to equation (9):

$$\begin{bmatrix} A_k^p \\ B_k^p \end{bmatrix} = -\frac{\mu_k^p}{\sqrt{Y^p}} \begin{bmatrix} \cosh(\bar{x}_a^p) & \sinh(\bar{x}_a^p) \\ \cosh(\bar{x}_b^p) & \sinh(\bar{x}_b^p) \end{bmatrix}^{-1} \begin{bmatrix} Y^p \dfrac{\mathrm{d}^2 w_k}{\partial \bar{x}^2}(\bar{x}_a^p) + (\lambda_k)^4 w_k(\bar{x}_a^p) \\ Y^p \dfrac{\mathrm{d}^2 w_k}{\partial \bar{x}^2}(\bar{x}_b^p) + (\lambda_k)^4 w_k(\bar{x}_b^p) \end{bmatrix}. \tag{11}$$

Now given the expression of $u_{1,k}^p$, the longitudinal shape $u_{3,k}$ of layer 3 may also be obtained from equation (2).

2.4. CORRESPONDING SHEAR DEFORMATION SHAPE

Recall equation (5) where the relationship between longitudinal and shear deformations is defined. Since $u_{1,k}^p$ is available now, the only unknown left is the constant s_k^p. Note that because s_k^p affects the shear strain energy, it is of importance here and it should be obtained from the energy viewpoint. The shear strain energy $U_{\gamma 2,k}^p$ of patch p in layer 2 is as follows where integration is carried out over the patch length from $\bar{x}_a^p$ to $\bar{x}_b^p$:

$$U_{\gamma 2,k}^p = \tfrac{1}{2} G_2 h_2^p l_x l_y \int_p (\gamma_{2,k}^p)^2 \, \mathrm{d}\bar{x}, \tag{12}$$

where G_2 is the shear modulus of layer 2, and l_y is the width of the beam. Substitute equations (5) and (9) into equation (12), minimize $U_{\gamma 2,k}^p$ by setting $\partial U_{\gamma 2,k}^p / \partial s_k^p = 0$ and subsequently find s_k^p as

$$\begin{aligned} s_k^p = \frac{(e^p+1)}{\bar{l}_x^p} \Bigg\{ & \frac{A_k^p}{\sqrt{Y^p}} [\cosh(\sqrt{Y^p}\bar{x}_b^p) - \cosh(\sqrt{Y^p}\bar{x}_a^p)] \\ & + \frac{B_k^p}{\sqrt{Y^p}} [\sinh(\sqrt{Y^p}\bar{x}_b^p) - \sinh(\sqrt{Y^p}\bar{x}_a^p)] \\ & + \left(\frac{C^p}{l_x(e^p+1)} + \mu_k^p Y^p \right) [w_k(\bar{x}_b^p) - w_k(\bar{x}_a^p)] \\ & + \mu_k^p \left[\frac{\mathrm{d}^3 w_k(\bar{x}_b^p)}{\mathrm{d}\bar{x}^3} - \frac{\mathrm{d}^3 w_k(\bar{x}_a^p)}{\mathrm{d}\bar{x}^3} \right] \Bigg\}. \end{aligned} \tag{13}$$

Now, the corresponding shear strain $\gamma_{2,k}^p$ of layer 2 is also available by combining equations (5) and (13).

2.5. NATURAL FREQUENCY AND MODAL LOSS FACTOR CALCULATIONS

With the availability of all deformation shapes, an energy formulation is used to estimate modal parameters of the sandwich beam for the kth mode of interest. The modal loss factor η_k is obtained as follows by using the modal strain energy method

$$\eta_k = \frac{\sum_{p=1}^{N_p} \eta_{m,2}^p U_{\gamma 2,k}^p}{U_{total,k}} \tag{14}$$

where $\eta_{m,2}^p$ is the material loss factor of the viscoelastic core of patch p and $U_{total,k}$ is the total modal strain energy that is approximated as

$$U_{total,k} = U_{w3,k} + \sum_{p=1}^{N_p} (U_{w1,k}^p + U_{u13,k}^p + U_{\gamma 2,k}^p). \tag{15}$$

Note that

$$U_{w3,k} = \frac{1}{2l_x^3} \int_0^1 E_3 I_3 \left(\frac{\mathrm{d}^2 w_k}{\mathrm{d}\bar{x}^2} \right)^2 \mathrm{d}\bar{x}, \qquad U_{w1,k}^p = \frac{1}{2l_x^3} \int_p E_1^p I_1^p \left(\frac{\mathrm{d}^2 w_k}{\mathrm{d}\bar{x}^2} \right)^2 \mathrm{d}\bar{x} \tag{16, 17}$$

are strain energies of layers 1 and 3 due to flexural motion, and

$$U_{u13,k}^p = \frac{1}{2l_x} E_1^p h_1^p l_y (1 + e^p) \int_p \left(\frac{\mathrm{d}u_{1,k}^p}{\mathrm{d}\bar{x}} \right)^2 \mathrm{d}\bar{x} \tag{18}$$

is the strain energy of layers 1 and 3 due to longitudinal motions. In addition, the undamped natural frequency is obtained by using the Rayleigh method:

$$\omega_k = \sqrt{U_{total,k}/T_{total,k}}, \tag{19}$$

where $T_{total,k}$ is the total kinetic energy of mode k. Again, $T_{total,k}$ is approximated based on flexural motion of all layers as

$$T_{total,k} \approx T_{w,k} = \tfrac{1}{2} l_x \int_0^1 \rho_3 I_3 (w_k)^2 \, \mathrm{d}\bar{x} + \tfrac{1}{2} l_x \sum_{p=1}^{N_p} \int_p (\rho_1^p I_1^p + \rho_2^p I_2^p)(w_k)^2 \, \mathrm{d}\bar{x}. \tag{20}$$

3. EXAMINATION OF APPROXIMATE METHOD I

3.1. PROCEDURE USING MEASURED OR COMPUTED MODE SHAPES

A practical beam structure may have mode shapes that differ from the ideal Euler beam eigenfunctions of section 2.1 due to non-classical boundary conditions, non-uniform geometry, and mass loading effects introduced by damping patches. In such cases, predicted (say from a finite element code) or measured flexural mode shapes of a sandwich beam may be obtained and then discreet spatial data are curve-fitted to yield a continuous function $\phi_{w,k}(\bar{x})$. In order to apply our method

to arbitrary mode shapes, $\phi_{w,k}(\bar{x})$ is approximated by a superposition of undamped Euler beam eigenfunctions $w_r(\bar{x})$ which are obtained by satisfying appropriate boundary conditions:

$$\phi_{w,k}(\bar{x}) = q_1 w_1(\bar{x}) + q_2 w_2(\bar{x}) + \cdots q_r w_r(\bar{x}) + \cdots \approx \sum_{r=1}^{N} q_r w_r(\bar{x}), \tag{21}$$

where N is the number of eigenfunctions included and q_r is the curve-fit coefficient. Taking advantage of the orthogonality relationships of Euler eigenfunctions, q_r is obtained as

$$q_r = \frac{\int_0^1 \phi_{w,k} w_r \, \mathrm{d}\bar{x}}{\int_0^1 (w_r)^2 \, \mathrm{d}\bar{x}}. \tag{22}$$

Following the superposition principle, the longitudinal $\phi_{u1,k}$ and shear $\phi_{\gamma 2,k}$ deformation are obtained as follows using equations (9) and (5):

$$\phi^p_{u1,k}(\bar{x}) = \sum_{r=1}^{N} q_r u^p_{1,r}(\bar{x}), \qquad \phi^p_{\gamma 2,k}(\bar{x}) = \sum_{r=1}^{N} q_r \gamma^p_{2,r}(\bar{x}). \tag{23, 24}$$

Replacing w_k, $u^p_{1,k}$ and $\gamma^p_{2,k}$ with $\phi_{w,k}$, $\phi^p_{u1,k}$ and $\phi^p_{\gamma 2,k}$ respectively in the energy equations (12, 16–18, 20), the natural frequency ω_k and modal loss factor η_k associated with a specific mode shape $\phi_{w,k}$ are obtained by using equations (14) and (19).

3.2. VALIDATION

A cantilever beam is used as an example to verify Approximate Method I in comparison with the analytical Rayleigh–Ritz method described earlier by the current authors in reference [1]. The beam and damping material parameters are summarized in Table 2. First, the full coverage case of Figure 4(a) is examined. The first five Euler beam eigenfunctions are assumed for the flexural displacements. Corresponding longitudinal and shear displacements are found, and modal strain and kinetic energies are obtained. Natural frequencies ω_k and modal loss factors η_k are then calculated using Approximate Method I. Predictions

TABLE 2

System parameters for the beam example

	Layer 1	Layer 2	Layer 3
Material	Steel	Viscoelastic	Steel
Stiffness (N/m^2)	$E_1 = 180 \times 10^9$	$G_2 = 0{\cdot}25 \times 10^6$	$E_3 = 180 \times 10^9$
Density (kg/m^3)	$\rho_1 = 7720$	$\rho_2 = 2000$	$\rho_3 = 7350$
Material loss factor	$\eta_{m,1} \ll \eta_{m,2}$	$\eta_{m,2} = 0{\cdot}1$	$\eta_{m,3} \ll \eta_{m,2}$
Dimensions			
Length (mm)	Varies	Varies	$l = 177{\cdot}8$
Thickness (mm)	$h_1 = 0{\cdot}79$	$h_2 = 0{\cdot}051$	$h_3 = 1{\cdot}47$

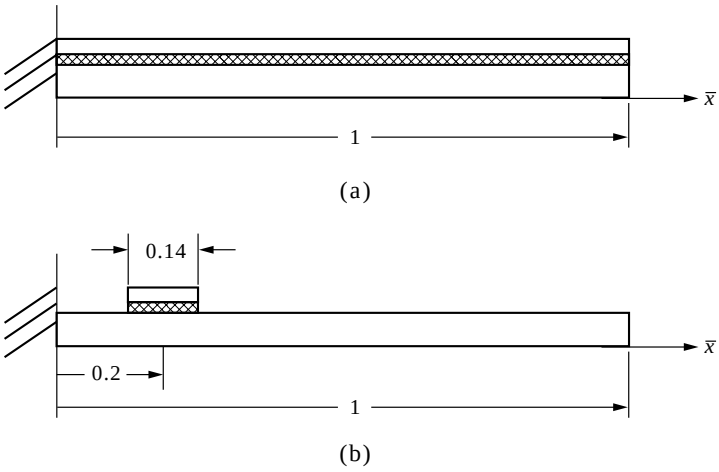

Figure 4. Cantilever beam examples: (a) full coverage, (b) partial coverage ($\bar{x}^p = 0{\cdot}2$, $\bar{l}^p = 0{\cdot}14$). Refer to Table 2 for parameters.

are listed in Table 3 in comparison with those obtained from the Rayleigh–Ritz method. It is seen that discrepancies are very small especially for higher modes. Discrepancies in modes 1 and 2 are larger because the actual mode shapes are different from the Euler beam eigenfunctions; this information can be found in Figure 16 of reference [1]. Thus, this method yields a good prediction only when the mode shape is correct.

Next, the same cantilever beam with a single patch of length $\bar{l}^p = 0{\cdot}14$ (Figure 4(b)) is examined and results are compared in Table 4. Due to the mass loading effect, actual mode shapes are expected to deviate more from the Euler beam eigenfunctions than those observed in the full coverage case. Therefore, larger discrepancies are observed. Finally the mode shapes are corrected by incorporating the mass loading effect and by expressing each mode as a superposition of the first 10 Euler beam eigenfunctions, using the formulation in

TABLE 3

Comparison between Rayleigh–Ritz method and Approximate Method I for the full coverage case. See Table 2 for parameters

	Modal loss factor (%)	
	Approximation I (with Euler beam mode description)	Rayleigh–Ritz Method
Mode 1	12·9	10·7
Mode 2	27·2	26·6
Mode 3	23·4	23·3
Mode 4	17·5	17·4
Mode 5	15·5	15·5

TABLE 4

Comparison between Rayleigh–Ritz method and Approximate Method I for the partial coverage (14%) *case using only one damping patch. See Table* 2 *for parameters*

	Modal loss factor (%)		
	Approximate Method I		
	With Euler beam mode description	With corrected mode shape*	Rayleigh–Ritz Method
Mode 1	0·20	0·16	0·16
Mode 2	0·01	0·01	0·01
Mode 3	0·22	0·25	0·26
Mode 4	0·74	0·72	0·72
Mode 5	0·88	0·73	0·73

* Superposition of Euler beam modes.

section 3.1; see Table 5 for typical values of curve-fit coefficients. Approximate Method I is now in excellent agreement with the Rayleigh–Ritz method, as evident from Table 4.

4. APPROXIMATE METHOD II FOR A COMPLIANT VISCOELASTIC CORE

4.1. FORMULATION

In many practical damping treatments, the viscoelastic layer is often very compliant compared with metallic layers (1 and 3). Consequently longitudinal deformations of elastic layers become negligible and Approximate Method I may be further simplified to yield Approximate Method II which calculates modal loss factors for a sandwich beam given arbitrary mode shapes. Recall equation (5)

TABLE 5

Curve-fit coefficients q_r for expressing mode shapes of the partially covered beam of Figure 4(*b*) *in terms of superposition of the undamped Euler beam eigenfunctions*

	Mode 1	Mode 2	Mode 3	Mode 4	Mode 5
q_1	1·0000	−0·0067	−0·0147	−0·0137	−0·0078
q_2	−0·0007	0·9999	−0·0691	−0·0604	−0·0356
q_3	0·0012	0·0082	0·9971	−0·1420	−0·0748
q_4	0·0010	0·0026	0·0260	0·9874	−0·1294
q_5	0·0005	0·0011	0·0042	0·0323	0·9877
q_6	0·0002	0·0005	0·0009	0·0044	0·0287
q_7	0·0000	0·0003	0·0009	0·0010	0·0042
q_8	−0·0001	0·0001	0·0011	0·0014	0·0008
q_9	−0·0001	0·0000	0·0008	0·0016	0·0008
q_{10}	−0·0001	−0·0001	0·0003	0·0010	0·0011

where $\gamma_{2,k}^p$ is determined from $u_{1,k}^p$, w_k, and s_k^p. The effect of $u_{1,k}^p$ on $\gamma_{2,k}^p$ is small when $G_2 \ll E_1$, compared with that of w_k. Note that s_k^p still needs to be determined by minimizing energy $U_{\gamma 2,k}^p$ irrespective of $u_{1,k}^p$. Then the shear deformation $\gamma_{2,k}^p$ is expressed in terms of w_k:

$$\gamma_{2,k}^p = \frac{C^p}{h_2^p l_x}\left[\frac{\mathrm{d}w_k(\bar{x})}{\mathrm{d}\bar{x}} - \frac{1}{\bar{l}_x^p} w_k(\bar{x}_b^p) + \frac{1}{\bar{l}_x^p} w_k(\bar{x}_a^p)\right]. \tag{25}$$

For a beam with arbitrary mode shape $\phi_{w,k}$, the shear deformation $\phi_{\gamma 2,k}^p$ is expressed by using equations (21, 24, 25):

$$\phi_{\gamma 2,k}^p = \frac{C^p}{h_2^p l_x}\left[\frac{\mathrm{d}\phi_{w,k}(\bar{x})}{\mathrm{d}\bar{x}} - \frac{1}{\bar{l}_x^p} \phi_{w,k}(\bar{x}_b^p) + \frac{1}{\bar{l}_x^p} \phi_{w,k}(\bar{x}_a^p)\right]. \tag{26}$$

Accordingly, the resulting shear strain energy is

$$U_{\gamma 2,k}^p = \frac{G_2 l_y (C^p)^2}{2h_2^p l_x} \int_p \left(\frac{\mathrm{d}\phi_{w,k}(\bar{x})}{\mathrm{d}\bar{x}} - \frac{1}{\bar{l}_x^p} \phi_{w,k}(\bar{x}_b^p) + \frac{1}{\bar{l}_x^p} \phi_{w,k}(\bar{x}_a^p)\right)^2 \mathrm{d}\bar{x}. \tag{27}$$

Replace w_k of equation (16) with $\phi_{w,k}$, ignore $U_{u13,k}^p$ in equation (15), and then apply equations (19) and (14) again to yield ω_k and η_k.

4.2. VALIDATION

Approximate Method II is validated by re-examining examples of Table 2 and Figure 4. For the full coverage case, loss factors for modes 2 and 3 are calculated over a range of G_2 values by using Methods I and II; comparisons are shown in Figure 5. It is observed that modal loss factors obtained from both methods coincide only when G_2 is very small. For the second mode when G_2 is greater than

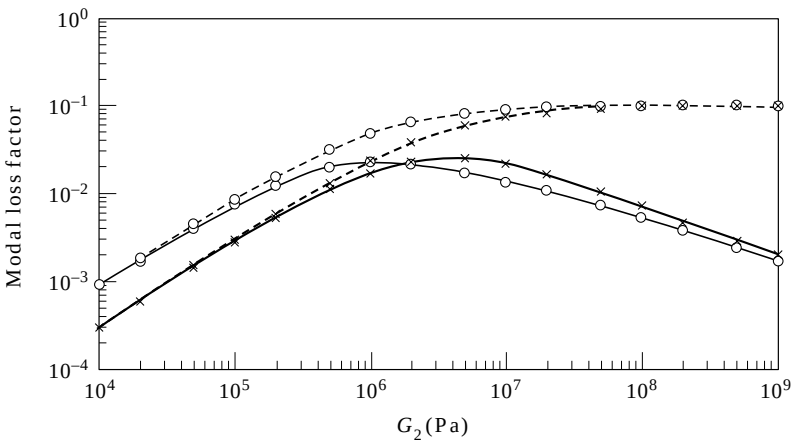

Figure 5. Modal loss factor predictions as a function of G_2 for the full coverage case. · · ·, Approximate Method I; ——, Approximate Method II; ○, mode 2; ×, mode 3.

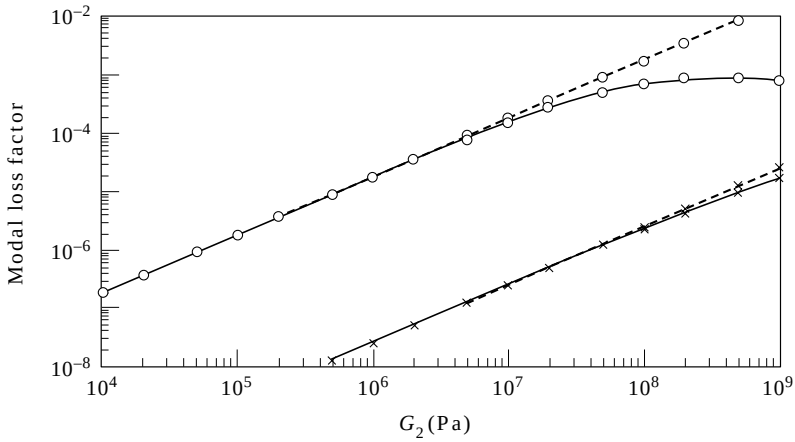

Figure 6. Loss factor predictions for mode 2 as a function of G_2 for partial coverage cases. · · ·, Approximate Method I; ——, Approximate Method II; ○, patch size $\bar{l}^p = 0{\cdot}14$; ×, patch size $\bar{l}^p = 0{\cdot}02$.

10^5 Pa, Method II starts to overestimate and finally the result asymptotically reaches 0·1, which is equal to the material loss factor of layer 2. Conversely, the lost factor prediction from Method I reaches a maximum value at $G_2 = G_{2,opt} = 10^6$ Pa and then reduces as G_2 is increased. Note that $G_{2,opt}$ is designated here as an optimum G_2 value that results in the maximum possible loss factor for a particular mode. Similar results are seen for mode 3 except that $G_{2,opt}$ now is about 3×10^6 Pa and Method II is valid up to $G_2 \approx 3 \times 10^6$ Pa using a 10% error criterion.

Next, consider the partial coverage case ($\bar{l}^p = 0{\cdot}14$) of Figure 4(b). Loss factors predicted for mode 2 are plotted in Figure 6. It is seen that $G_{2,opt}$ shifts to a higher value and Method II is now valid up to $G_2 = 5 \times 10^6$ Pa. This suggests that Method II may be used up to higher G_2 values for even smaller patches. Another partial coverage case with a compact patch of $\bar{l}^p = 0{\cdot}02$ applied at the same location shows that Method II is indeed valid up to $G_2 = 2 \times 10^8$ Pa. Consequently the very compliant core assumption of Method II is not necessary when a very compact patch is applied.

5. APPROXIMATE METHOD III FOR A COMPACT PATCH

5.1. FORMULATION

Consider a compact patch of very small patch length $\bar{l}_x^p$. Expand $\mathrm{d}\phi_{w,k}(\bar{x})/\mathrm{d}\bar{x}$ using the Taylor series in the vicinity of the patch center $\bar{x}_p$, and obtain the following expression by ignoring higher order terms:

$$\frac{\mathrm{d}\phi_{w,k}(\bar{x})}{\mathrm{d}\bar{x}} \approx \frac{\mathrm{d}\phi_{w,k}(\bar{x}^p)}{\mathrm{d}\bar{x}} + \frac{\mathrm{d}^2\phi_{w,k}(\bar{x}^p)}{\mathrm{d}\bar{x}^2}(\bar{x} - \bar{x}^p). \tag{28}$$

Also, observe that

$$\frac{\mathrm{d}\phi_{w,k}(\bar{x}^p)}{\mathrm{d}\bar{x}} \approx \frac{1}{\bar{l}^p}\left[\phi_{w,k}(\bar{x}_b^p) - \phi_{w,k}(\bar{x}_a^p)\right]. \tag{29}$$

Substituting equations (28) and (29) into (27), the resulting shear strain energy for the kth mode is

$$U_{\gamma 2,k}^p \approx \frac{G_2 l_y (C^p)^2}{2h_2^p l_x}\left(\frac{\mathrm{d}^2\phi_{w,k}(\bar{x}^p)}{\mathrm{d}\bar{x}^2}\right)^2 \int_{\bar{x}_a^p}^{\bar{x}_b^p} (\bar{x} - \bar{x}^p)^2\,\mathrm{d}\bar{x}$$

$$= \frac{G_2 l_y (C^p)^2}{2h_2^p l_x}\left(\frac{\mathrm{d}^2\phi_{w,k}(\bar{x}^p)}{\mathrm{d}\bar{x}^2}\right)^2 \frac{(\bar{l}_x^p)^3}{12}. \tag{30}$$

Similar to equation (14), the modal loss factor η_k^p contributed by a compact patch p is expressed by using the modal strain energy method:

$$\eta_k^p = \eta_{m,2}^p U_{\gamma 2,k}^p / U_{total,k}. \tag{31}$$

Further approximate the total strain energy of equation ($U_{total,k}$) by the flexural strain energy of the base beam ($U_{w3,k}$). The modal loss factor η_k^p is then evaluated by using equations (30) and (31):

$$\eta_k^p = \eta_{m,2}^p \mathscr{G}^p \mathscr{H}^p \mathscr{L}^p \hat{\mathscr{P}}(\bar{x}^p), \tag{32}$$

where

$$\mathscr{G}^p = G_2^p/E_3 = \text{relative stiffness term}, \tag{33a–f}$$

$$\mathscr{H}^p = (C^p)^2/(h_3^3 h_2^p) = \text{thickness parameter},$$

$$\mathscr{L}^p = (\bar{l}^p)^3 = \text{patch size index}, \quad \mathscr{P}(\bar{x}) = \left(\frac{\mathrm{d}^2\phi_{w,k}(\bar{x})}{\mathrm{d}\bar{x}^2}\right)^2 = \text{patch performance index},$$

$$\hat{\mathscr{P}}(\bar{x}) = \frac{\mathscr{P}(\bar{x})}{\mathscr{P}_0} = \text{normalized } \mathscr{P}(\bar{x}), \qquad \mathscr{P}_0 = \int_0^1 \left(\frac{\mathrm{d}^2\phi_{w,k}(\bar{x})}{\mathrm{d}\bar{x}^2}\right)^2 \mathrm{d}\bar{x}.$$

5.2. VALIDATION STUDIES

As described in the derivation of Method III, equations (31) and (32) can now be used to conduct parametric design studies and to determine optimum patch locations. The procedure is demonstrated here using the same beam example of Table 2.

First, examine the second mode (Figure 7(a)) of the beam with simply supported boundary conditions. The normalized patch index $\hat{\mathscr{P}}$ is calculated for mode 2 as a function of $\bar{x}$ as shown in Figure 7(b). High values of $\hat{\mathscr{P}}$ ($\bar{x}_{max} = 0{\cdot}25$ and $\bar{x}_{max} = 0{\cdot}75$) suggest the best patch locations that should result in high modal damping. This is in agreement with an empirical design concept: place damping patches at anti-nodes. To verify this, a compact patch of length $\bar{l}^p = 0{\cdot}1$ is placed

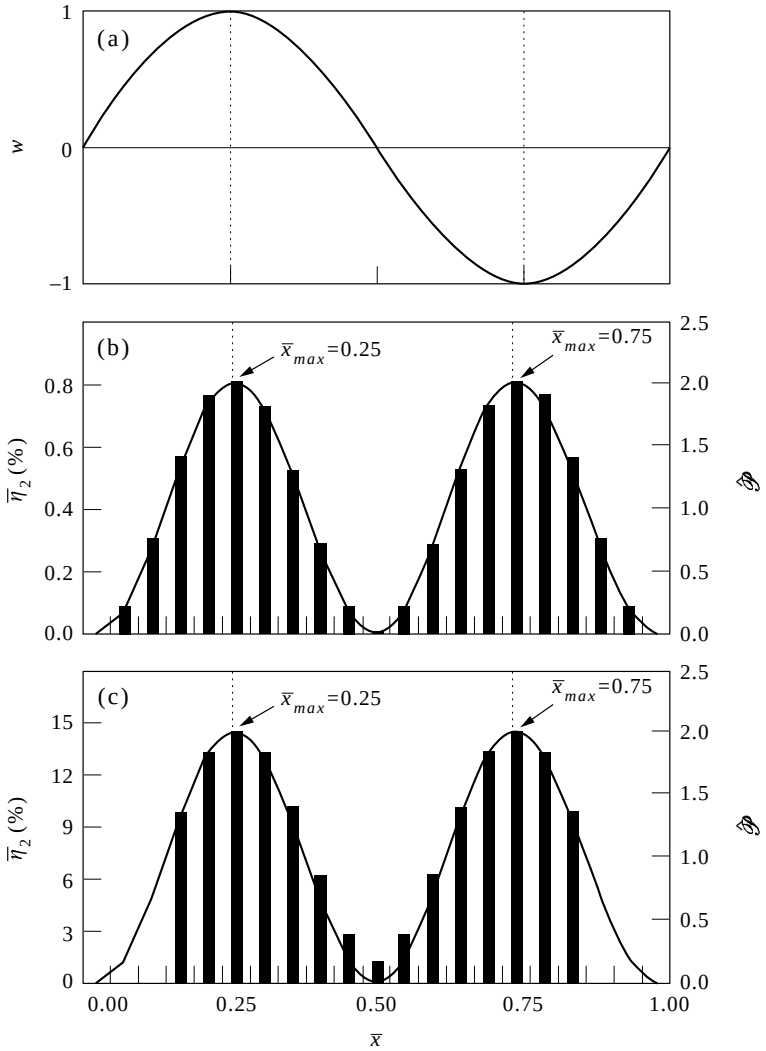

Figure 7. Patch performance for the second mode of a simply supported beam when a compact patch is placed at various $\bar{x}$. (a) Mode shape, (b) $\bar{l}^p = 0.1$, (c) $\bar{l}^p = 0.3$). Here $\bar{x}_{max}$ is the location that yields maximum possible $\bar{\eta}_2$. ——, Normalized patch performance index $\hat{\mathscr{P}}$; ■, predicted $\bar{\eta}_2$.

at various position $\bar{x}$ along the beam. Modal loss factors are calculated using the Rayleigh–Ritz method [1] and then normalized with respect to the full coverage case. Observe excellent agreement between the patch performance index and the Rayleigh–Ritz method. This demonstrates that the patch locations suggested by Method III are appropriate. Further, apply a larger patch of length $\bar{l}^p = 0{\cdot}3$ and calculate normalized modal loss factors of the beam with varying patch location using the Rayleigh–Ritz method. Figure 7(c) again shows excellent agreement except for the case when the patch is placed at $\bar{x}_{min} = 0{\cdot}5$. This discrepancy is due to the compact patch assumption of Method III and $\hat{\mathscr{P}}(\bar{x}_{min})$ is virtually zero; however, the modal loss factor is non-zero for a larger patch even when the patch

is located at $\bar{x}_{min}$. Therefore, Method III should be viewed as an analytical tool for initiating design.

Next, the second mode of the cantilever beam is examined, as shown in Figure 8(a). The normalized patch index $\hat{\mathscr{P}}$ is calculated for mode 2 as a function of $\bar{x}$, as shown in Figure 8(b). It is then compared with measured and predicted (using Method I) $\bar{\eta}_2$ for the cantilever beam with a patch of length $\bar{l}^p = 0{\cdot}14$ placed at various positions $\bar{x}$. Excellent agreement is again observed between Methods I, III and modal measurements [1]. But note that the empirical design concept of placing damping patches at anti-nodes is not exactly valid for this case. It is seen in Figure 8(a) that the anti-node of mode 2 is located at $\bar{x}_{max} = 0{\cdot}48$. However,

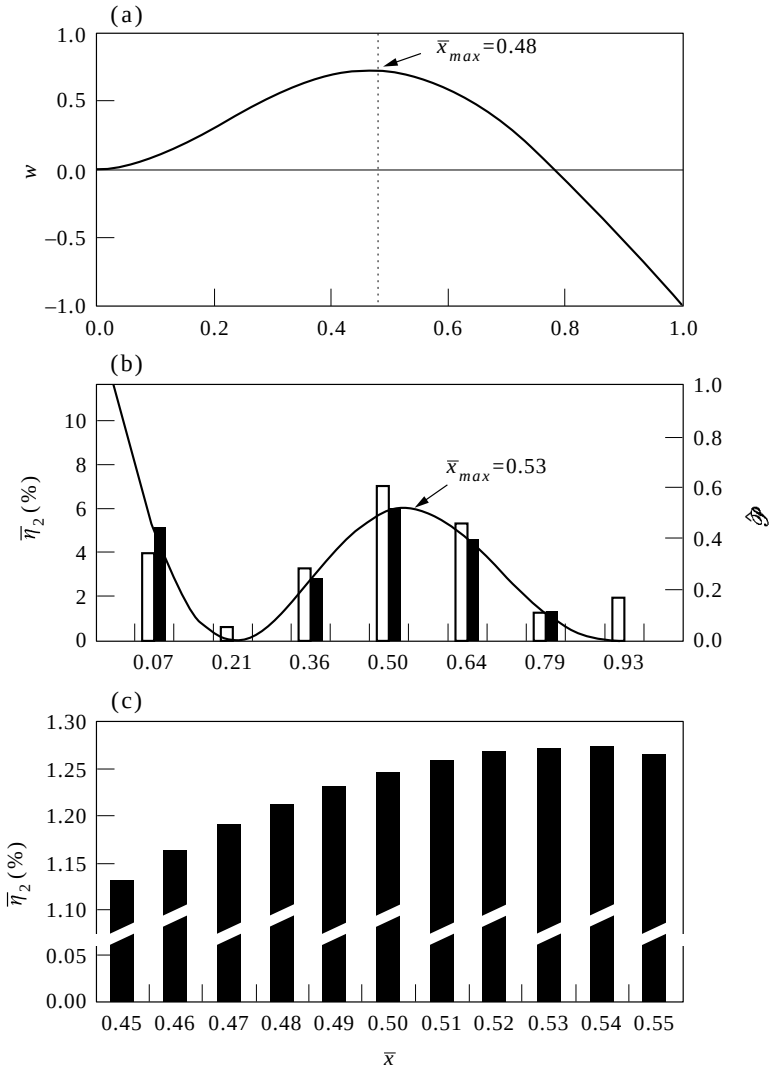

Figure 8. Comparison between patch performance index and Rayleigh–Ritz predictions for the second mode of a cantilever beam when a single patch of length $\bar{l}^p = 0.14$ is placed at various $\bar{x}$. (a) Mode shape, (b) comparison between Methods I, III, and experiment, (c) Rayleigh–Ritz predictions. ——, Normalized patch performance index $\hat{\mathscr{P}}$; □, measured $\bar{\eta}_2$; ■, predicted $\bar{\eta}_2$.

according to the patch index, one of the relative maxima of $\hat{\mathscr{P}}$ is at $\bar{x}_{max} = 0{\cdot}53$. It is then verified by using the Rayleigh–Ritz method. The placement of the damping patch at $\bar{x} = 0{\cdot}53$ gives higher modal damping than at $\bar{x} = 0{\cdot}48$ (Figure 8(c)). For higher modes, the high $\hat{\mathscr{P}}$ point is closer to an anti-node since such modes are less affected by the precise nature of boundary conditions. Hence, insight based on simple supports may be a good starting point for design, but then Method I or II may be used for detailed studies. Also note that another relative maximum at $\bar{x}_{max} = 0$ is observed in Figure 8(b). Since it is impossible to place a patch of finite length $\bar{l}^p$ at $\bar{x} = 0$ without exceeding the beam, the patch may be located near the root to obtain high damping performance.

6. APPROXIMATE METHODS FOR RECTANGULAR PLATES

6.1. APPROXIMATE METHOD II GIVEN MEASURED OR COMPUTED MODE SHAPES

Approximate Method II for beams with a compliant core layer assumption (as presented in section 4) is now extended to a 2-D case. The structure of interest is a rectangular plate with multiple damping patches, as illustrated in Figure 9. Assume that the measured or computed mode shape $\phi_{w,k}(\bar{x}, \bar{y})$ is available. The shear strain $\phi^p_{\gamma x2,k}$ in the xz plane of layer 2 is approximated as follows when longitudinal motion is ignored

$$\phi^p_{\gamma x2,k} = \frac{C^p}{h_2 l_x}\left[\frac{\mathrm{d}\phi_{w,k}(\bar{x}, \bar{y})}{\mathrm{d}\bar{x}} - \frac{1}{\bar{l}^p_x \bar{l}^p_y}\iint\limits_p \frac{\mathrm{d}\phi_{w,k}(\bar{x}, \bar{y})}{\mathrm{d}x}\,\mathrm{d}\bar{x}\,\mathrm{d}\bar{y}\right]. \tag{34}$$

Then the strain energy $U^p_{\gamma x2,k}$ due to $\phi^p_{\gamma x2,k}$ is obtained as

$$U^p_{\gamma x2,k} = \frac{G^p_2 l_y (C^p)^2}{2h^p_2 l_x}\left\{\iint\limits_p\left[\frac{\mathrm{d}\phi_{w,k}(\bar{x}, \bar{y})}{\mathrm{d}\bar{x}}\right]^2 \mathrm{d}\bar{x}\,\mathrm{d}\bar{y} - \frac{1}{\bar{l}^p_x \bar{l}^p_y}\left[\iint\limits_p \frac{\mathrm{d}\phi_{w,k}(\bar{x}, \bar{y})}{\mathrm{d}\bar{x}}\,\mathrm{d}\bar{x}\,\mathrm{d}\bar{y}\right]^2\right\}. \tag{35}$$

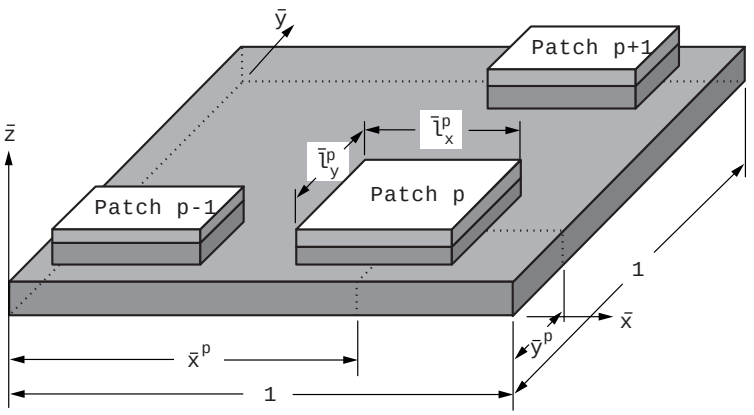

Figure 9. Multiple constrained layer damping patches for a rectangular plate.

Similarly, the shear strain $\phi^p_{\gamma y2,k}$ in the yz plane of layer 2 and its resulting strain energy $U^p_{\gamma y2,k}$ are

$$\phi^p_{\gamma x2,k} = \frac{C^p}{h^p_2 l_y}\left[\frac{\mathrm{d}\phi_{w,k}(\bar{x},\bar{y})}{\mathrm{d}\bar{y}} - \frac{1}{\bar{l}^p_x \bar{l}^p_y}\iint_p \frac{\mathrm{d}\phi_{w,k}(\bar{x},\bar{y})}{\mathrm{d}\bar{y}}\,\mathrm{d}\bar{x}\,\mathrm{d}\bar{y}\right],$$

$$U^p_{\gamma y2,k} = \frac{G_2 l_x (C^p_y)^2}{2h^p_2 l_y}\left\{\iint_p\left[\frac{\mathrm{d}\phi_{w,k}(\bar{x},\bar{y})}{\mathrm{d}\bar{y}}\right]^2 \mathrm{d}\bar{x}\,\mathrm{d}\bar{y} - \frac{1}{\bar{l}^p_x \bar{l}^p_y}\left[\iint_p \frac{\mathrm{d}\phi_{w,k}(\bar{x},\bar{y})}{\mathrm{d}\bar{y}}\,\mathrm{d}\bar{x}\,\mathrm{d}\bar{y}\right]^2\right\}. \tag{36}$$

Again, the total strain energy $U_{total,k}$ is approximated as

$$U_{total,k} = U_{w3,k} + \sum_{p=1}^{N_p}(U^p_{w1,k} + U^p_{\gamma x2,k} + U^p_{\gamma y2,k}), \tag{37}$$

where $U^p_{w1,k}$ and $U_{w3,k}$ are strain energies due to the flexural motion, defined as

$$U^p_{w1,k} = \tfrac{1}{2} l_x l_y \frac{E^p_1 (h^p_1)^3}{12[1-(v^p_1)^2]}\iint_p\left[\frac{1}{l^4_x}\left(\frac{\mathrm{d}^2\phi_{w,k}}{\mathrm{d}\bar{x}^2}\right)^2 + \frac{1}{l^4_y}\left(\frac{\mathrm{d}^2\phi_{w,k}}{\mathrm{d}\bar{y}^2}\right)^2 + \frac{2v^p_1}{l^2_x l^2_y}\left(\frac{\mathrm{d}^2\phi_{w,k}}{\mathrm{d}\bar{x}^2}\right)\left(\frac{\mathrm{d}^2\phi_{w,k}}{\mathrm{d}\bar{y}^2}\right) + \frac{2(1-v^p_1)}{l^2_x l^2_y}\left(\frac{\mathrm{d}^2\phi_{w,k}}{\mathrm{d}\bar{x}\,\mathrm{d}\bar{y}}\right)^2\right]\mathrm{d}\bar{x}\,\mathrm{d}\bar{y}, \tag{38}$$

$$U^p_{w3,k} = \tfrac{1}{2} l_x l_y \frac{E_3 (h_3)^3}{12[1-(v_3)^2]}\int_0^1\int_0^1\left[\frac{1}{l^4_x}\left(\frac{\mathrm{d}^2\phi_{w,k}}{\mathrm{d}\bar{x}^2}\right)^2 + \frac{1}{l^4_y}\left(\frac{\mathrm{d}^2\phi_{w,k}}{\mathrm{d}\bar{y}^2}\right)^2 + \frac{2v_3}{l^2_x l^2_y}\left(\frac{\mathrm{d}^2\phi_{w,k}}{\mathrm{d}\bar{x}^2}\right)\left(\frac{\mathrm{d}^2\phi_{w,k}}{\mathrm{d}\bar{y}^2}\right) + \frac{2(1-v_3)}{l^2_x l^2_y}\left(\frac{\mathrm{d}^2\phi_{w,k}}{\mathrm{d}\bar{x}\,\mathrm{d}\bar{y}}\right)^2\right]\mathrm{d}\bar{x}\,\mathrm{d}\bar{y}. \tag{39}$$

Finally, η_k is obtained by using the modal strain energy method per equation (14).

6.2. APPROXIMATE METHOD III

Similar to the discussion of section 5.1, compact patches of very small lengths $\bar{l}^p_x$ and widths $\bar{l}^p_y$ are assumed, and $\mathrm{d}\phi_{w,k}(\bar{x},\bar{y})/\mathrm{d}\bar{x}$ is again expanded using the Taylor series where the third and higher order terms are ignored:

$$\frac{\mathrm{d}\phi_{w,k}(\bar{x},\bar{y})}{\mathrm{d}\bar{x}} \approx \frac{\mathrm{d}\phi_{w,k}(\bar{x}^p,\bar{y})}{\mathrm{d}\bar{x}} + \frac{\mathrm{d}^2\phi_{w,k}(\bar{x}^p,\bar{y})}{\mathrm{d}\bar{x}^2}(\bar{x}-\bar{x}^p). \tag{40}$$

Also observing that

$$\frac{\mathrm{d}\phi_{w,k}(\bar{x}^p,\bar{y})}{\mathrm{d}\bar{x}} \approx \frac{1}{\bar{l}^p_x \bar{l}^p_y}\iint_p \frac{\mathrm{d}\phi_{w,k}(\bar{x},\bar{y})}{\mathrm{d}\bar{x}}\,\mathrm{d}\bar{x}\,\mathrm{d}\bar{y}, \tag{41}$$

the resulting shear strain energy $U^p_{\gamma x2,k}$ is approximated as

$$U^p_{\gamma x2,k} = \frac{G^p_2 l_y (C^p)^2}{2h^p_2 l_x}\left[\frac{\mathrm{d}^2\phi_{w,k}(\bar{x}^p, \bar{y}^p)}{\mathrm{d}\bar{x}^2}\right]^2 \frac{\bar{l}^p_y(\bar{l}^p_x)^3}{12}. \tag{42}$$

Similarly, shear strain energy $U^p_{\gamma y2,k}$ is approximated as

$$U^p_{\gamma y2,k} = \frac{G^p_2 l_x (C^p)^2}{2h^p_2 l_y}\left[\frac{\mathrm{d}^2\phi_{w,k}(\bar{x}^p, \bar{y}^p)}{\mathrm{d}\bar{y}^2}\right]^2 \frac{\bar{l}^p_x(\bar{l}^p_y)^3}{12}. \tag{43}$$

Ignoring flexural strain energy due to the damping patch, a general expression of the loss factor like equation (31) for beams is proposed as

$$\eta^p_k = \eta^p_{m,2}\mathscr{G}^p\mathscr{H}^p[\mathscr{L}^p_x\hat{\mathscr{P}}_x(\bar{x}^p, \bar{y}^p) + \mathscr{L}^p_y\hat{\mathscr{P}}_y(\bar{x}^p, \bar{y}^p)], \tag{44}$$

where $\mathscr{L}^p_x$ is the patch size index, and $\hat{\mathscr{P}}_x$ is the normalized patch performance index associated with shear strains $\phi^p_{\gamma x2,k}$. Similarly indices $\mathscr{L}^p_y$ and $\hat{\mathscr{P}}_y$ are associated with shear strains $\phi^p_{\gamma x2,k}$. In addition, the thickness parameter $\mathscr{H}^p = (C^p)^2/(h^3_3 h^p_2)$ is the same as in section 5.1 while the relative stiffness $\mathscr{G}^p$ term is now equal to $G^p_2(1 - v^2_3)/E_3$. The patch size indices, $\mathscr{L}^p_x$ and $\mathscr{L}^p_y$, are obtained as

$$\mathscr{L}^p_x = \bar{l}^p_y(\bar{l}^p_x)^3, \qquad \mathscr{L}^p_y = \bar{l}^p_x(\bar{l}^p_y)^3. \tag{45}$$

Patch performance indices and their normalized forms are

$$\mathscr{P}_x(\bar{x}, \bar{y}) = \left(\frac{\mathrm{d}^2\phi_{w,k}(\bar{x}, \bar{y})}{l^2_x\,\mathrm{d}\bar{x}^2}\right)^2; \qquad \mathscr{P}_y(\bar{x}, \bar{y}) = \left(\frac{\mathrm{d}^2\phi_{w,k}(\bar{x}, \bar{y})}{l^2_y\,\mathrm{d}\bar{y}^2}\right)^2,$$

$$\hat{\mathscr{P}}_x(\bar{x}, \bar{y}) = \frac{\mathscr{P}_x(\bar{x}, \bar{y})}{\mathscr{P}_0}; \qquad \hat{\mathscr{P}}_y(\bar{x}, \bar{y}) = \frac{\mathscr{P}_y(\bar{x}, \bar{y})}{\mathscr{P}_0}, \tag{46a–d}$$

TABLE 6

System parameters for the rectangular plate example

	Layer 1*	Layer 2*	Layer 3
Material			
Stiffness (N/m^2)	$E_1 = 180 \times 10^9$	$G_2 = 0{\cdot}25 \times 10^6$	$E_3 = 180 \times 10^9$
Poisson's ratio	$v_1 = 0{\cdot}3$	$v_2 = 0{\cdot}45$	$v_3 = 0{\cdot}3$
Density (kg/m^3)	$\rho_1 = 7720$	$\rho_2 = 2000$	$\rho_3 = 7350$
Material loss factor	$\eta_{m,1} \ll \eta_{m,2}$	$\eta_{m,2} = 0{\cdot}8$	$\eta_{m,3} \ll \eta_{m,2}$
Dimensions			
Length (mm)	Varies	Varies	$l_x = 342{\cdot}9$
Width (mm)	Varies	Varies	$l_y = 266{\cdot}7$
Thickness (mm)	$\eta_1 = 0{\cdot}79$	$\eta_2 = 0{\cdot}051$	$\eta_3 = 2{\cdot}4$

* Material provided by the Wolverine Gasket Company; Code: WXP-1828.

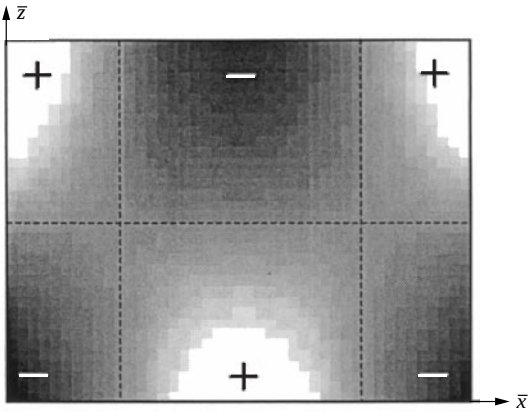

(a)

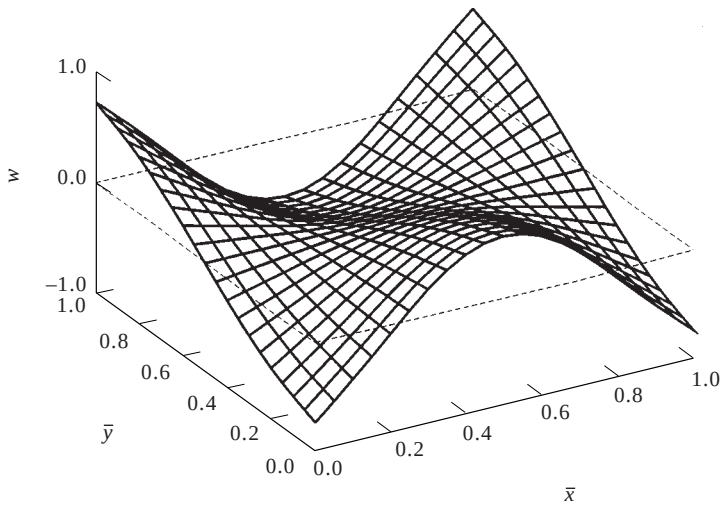

(b)

Figure 10. Deformation shape of mode (2, 1) of a rectangular plate with free boundaries. Dotted lines represent nodal lines. (a) 2-D plot, (b) 3-D plot.

where

$$\mathscr{P}_0 = \int_0^1 \int_0^1 \left[\frac{1}{l_x^4} \left(\frac{\mathrm{d}^2 \phi_{w,k}}{\mathrm{d}\bar{x}^2} \right)^2 + \frac{1}{l_y^4} \left(\frac{\mathrm{d}^2 \phi_{w,k}}{\mathrm{d}\bar{y}^2} \right)^2 \right.$$

$$\left. + \frac{2\nu_3}{l_x^2 l_y^2} \left(\frac{\mathrm{d}^2 \phi_{w,k}}{\mathrm{d}\bar{x}^2} \right) \left(\frac{\mathrm{d}^2 \phi_{w,k}}{\mathrm{d}\bar{y}^2} \right) + \frac{2(1-\nu_3)}{l_x^2 l_y^2} \left(\frac{\mathrm{d}^2 \phi_{w,k}}{\mathrm{d}\bar{x}\, \mathrm{d}\bar{y}} \right)^2 \right] \mathrm{d}\bar{x}\, \mathrm{d}\bar{y}. \tag{47}$$

Finally, define the combined patch performance index $\mathscr{P}$ and its normalized value $\hat{\mathscr{P}}$ as follows to quantify the global effect of damping but only for a specific mode, over the entire surface of vibrating plate:

$$\mathscr{P}(\bar{x}, \bar{y}) = \mathscr{P}_x(\bar{x}, \bar{y}) + \mathscr{P}_y(\bar{x}, \bar{y}), \qquad \hat{\mathscr{P}}(\bar{x}, \bar{y}) = \hat{\mathscr{P}}_x(\bar{x}, \bar{y}) + \hat{\mathscr{P}}_y(\bar{x}, \bar{y}). \quad \text{(48a, b)}$$

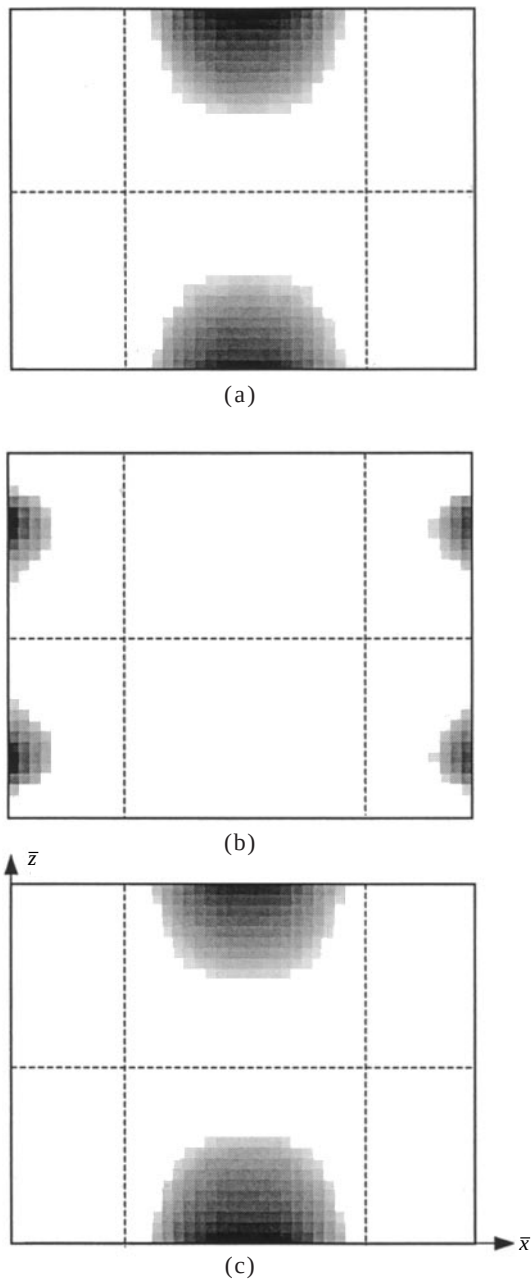

Figure 11. The (2, 1) mode shape and corresponding patch performance indices for the plate example of Table 6 with free boundaries. (a) Flexural mode ϕ_w, (b) $\mathscr{P}_x$, (c) $\mathscr{P}_y$, (d) $\mathscr{P}$.

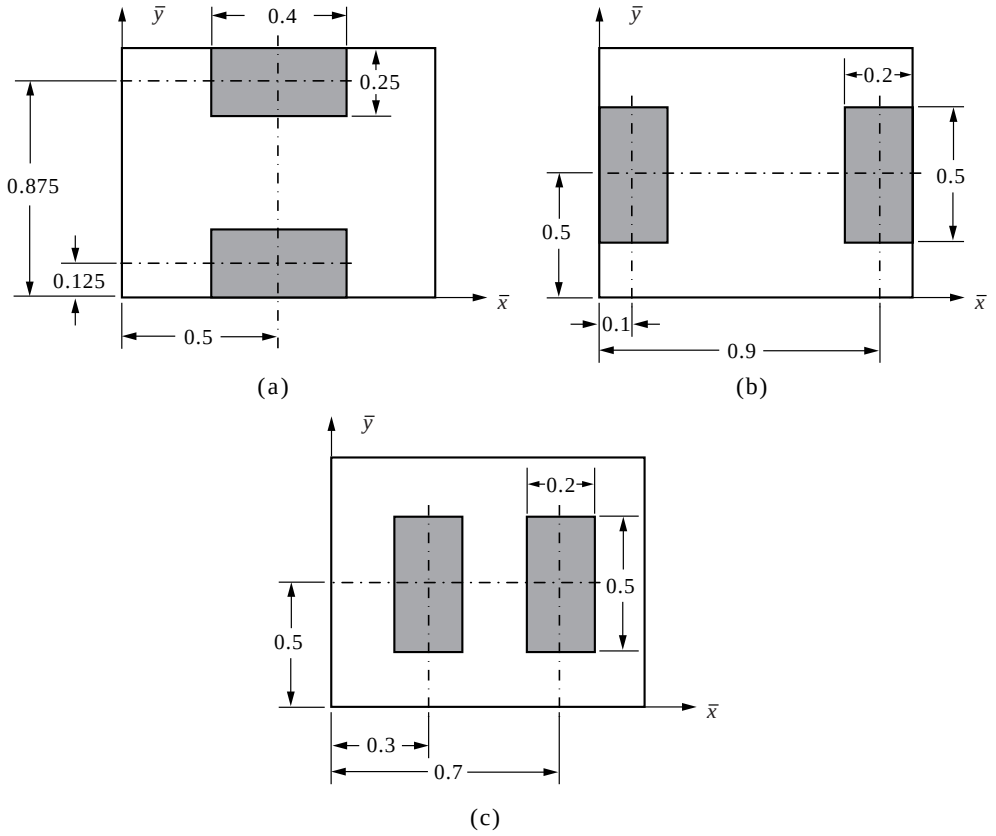

Figure 12. Damping patch configurations studied for the rectangular plate example of Table 6 with free boundaries. (a) Pattern A, (b) Pattern B, (c) Pattern C.

7. EXAMINATION OF PLATE FORMULATIONS

7.1. VALIDATION STUDIES

A rectangular plate with free boundary at all edges is considered here for experimental verification. System parameters of the plate and the damping patches are summarized in Table 6. The undamped mode shapes are calculated using a Rayleigh–Ritz method [2] prior to the application of Method III. In particular, mode (2, 1), as shown in Figure 10 is considered for the sake of illustration. As seen in Figures 11(a) and (b), the patch performance indices $\mathscr{P}_x$ and $\mathscr{P}_y$ are calculated over the plate surface respectively from the undamped mode shape. Note that the dark areas imply high $\mathscr{P}_x$ or $\mathscr{P}_y$ values; these suggest locations that should result in high damping performance. Since $\mathscr{P}_x$ is about one order of magnitude higher than $\mathscr{P}_y$, the combined index $\mathscr{P}$ of Figure 11(c) is dominated by $\mathscr{P}_x$. Consider a preliminary design: cover the dark areas of $\mathscr{P}$ by applying two identical damping patches of $\bar{l}_x^p = 0{\cdot}4$ and $\bar{l}_y^p = 0{\cdot}25$ and locate them at $(\bar{x}, \bar{y}) = (0{\cdot}5, 0{\cdot}125)$ and $(0{\cdot}5, 0{\cdot}875)$, as shown in Figure 12(a). This configuration is designated as Pattern A. Two alternate configurations, designated as Patterns B and C, are also considered in Figures 12(b) and (c), respectively. Predicted modal loss factors for all three cases are then obtained using Approximate Methods II

TABLE 7

Comparison between measured and predicted modal loss factors for the rectangular plate of Figure 10 *with free boundaries. See Table* 6 *for parameters*

	Loss factor for mode (2, 1) (%)			
		Theory		
Damping patch	Experiment	Rayleigh–Ritz Method	Approximate Method II	Approximate Method III
Pattern A	1·9	1·5	1·7	2·0
Pattern B	1·3	1·2	1·4	0·0
Pattern C	0·7	0·7	0·9	0·0

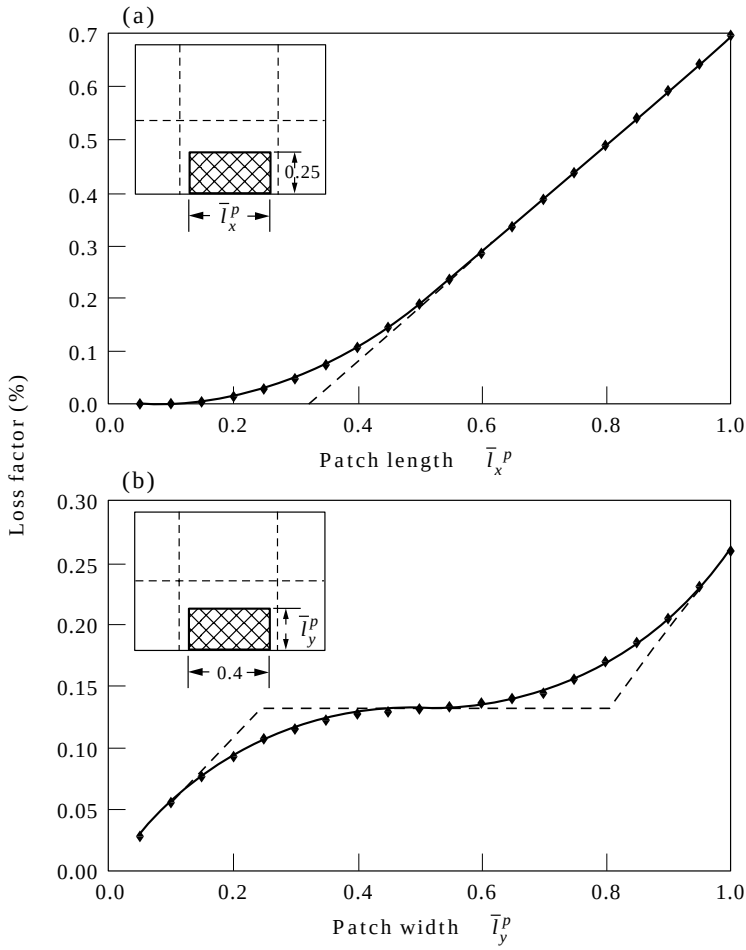

Figure 13. Effect of patch dimensions for the rectangular plate of Table 6 with free boundaries. (a) Varying patch length, (b) varying patch width. —◆—, Prediction, ---, asymptote.

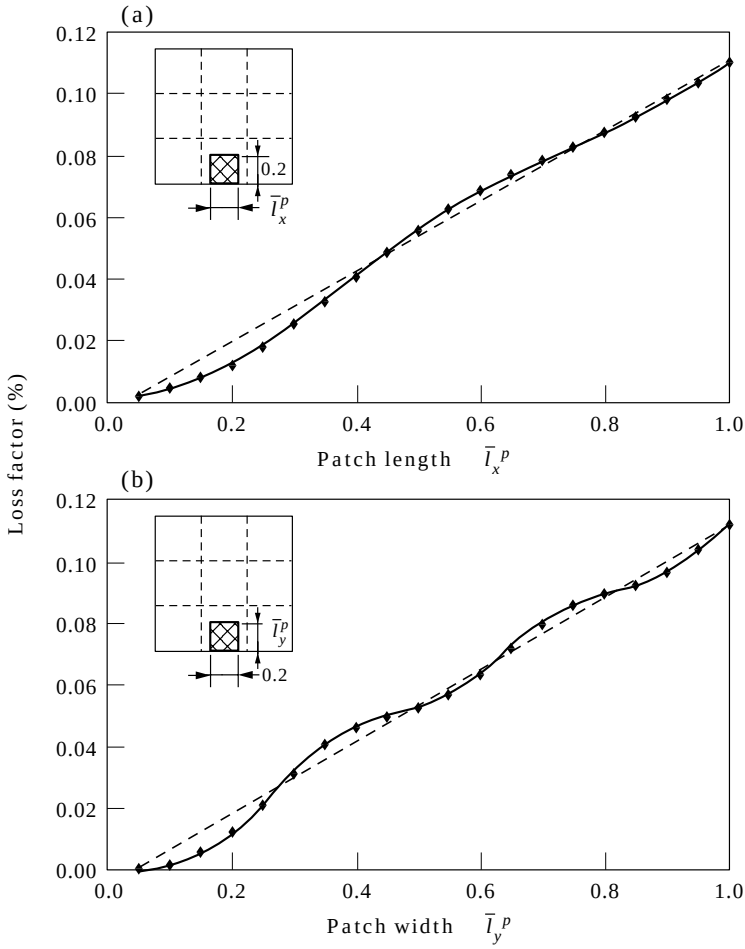

Figure 14. Effect of patch dimensions for the rectangular plate of Table 6 with simply supported edges. (a) Varying patch length, (b) varying patch width. —◆—, Prediction, ---, asymptote.

and III. These are compared with modal measurements [2] and Rayleigh–Ritz predictions in Table 7. Results indicate that Pattern A indeed yields the highest system damping for this particular mode. Observe an excellent agreement between theory and experiment which confirms the utility of Method II. Also note that Table 7 suggests that modal loss factors for Patterns B and C are zero only when Method III is used for prediction. This is because both $\mathscr{P}_x$ and $\mathscr{P}_y$ are zero for patches located along the line of $\bar{l}_y = 0{\cdot}5$; this is similar to the discussion of $\hat{\mathscr{P}}(\bar{x}_{min}) = 0$ in section 5.2.

7.2. PARAMETRIC STUDIES

Effects of patch lengths and widths are investigated next by using Approximate Method II. Consider only one patch and locate it at $(\bar{x}, \bar{y}) = (0{\cdot}5, 0{\cdot}125)$. Fix width as $\bar{l}_y^p = 0{\cdot}25$ and vary axial length $\bar{l}_x^p$ from 0 to 1. It is seen from Figure 13(a) that the loss factor for mode (2, 1) increases as the patch length is increased and the relationship gradually becomes linear as the asymptotic curve suggests. Then, fix

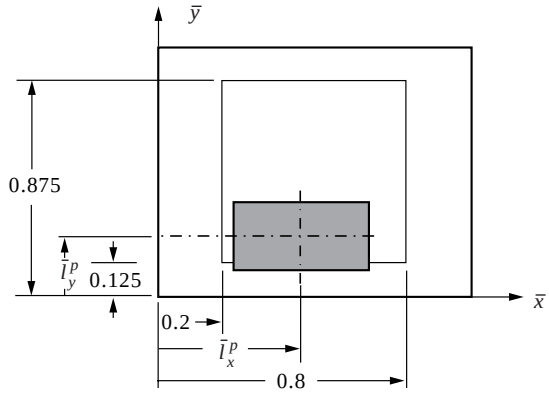

Figure 15. Possible patch locations on the rectangular plate with free boundaries for a detailed parametric study.

length $\bar{l}_x^p = 0{\cdot}4$ and vary the patch width $\bar{l}_y^p$ from 0 to 1. Figure 13(b) shows that η varies linearly first, then settles down when $\bar{l}_y^p$ is greater than 0·3, and finally increases for $\bar{l}_y^p > 0{\cdot}7$. Three asymptotic lines approximate the curve rather well. The flat asymptotic line also reflects the low $\mathscr{P}$ region of Figure 11(c) at the center of the plate; this is an inefficient location for a damping patch.

Such asymptotic results are rather problem specific, as evident from yet another example of Figure 14 where a simply supported square plate is considered. Material properties of the patches and plate of Table 6 are the same as the previous

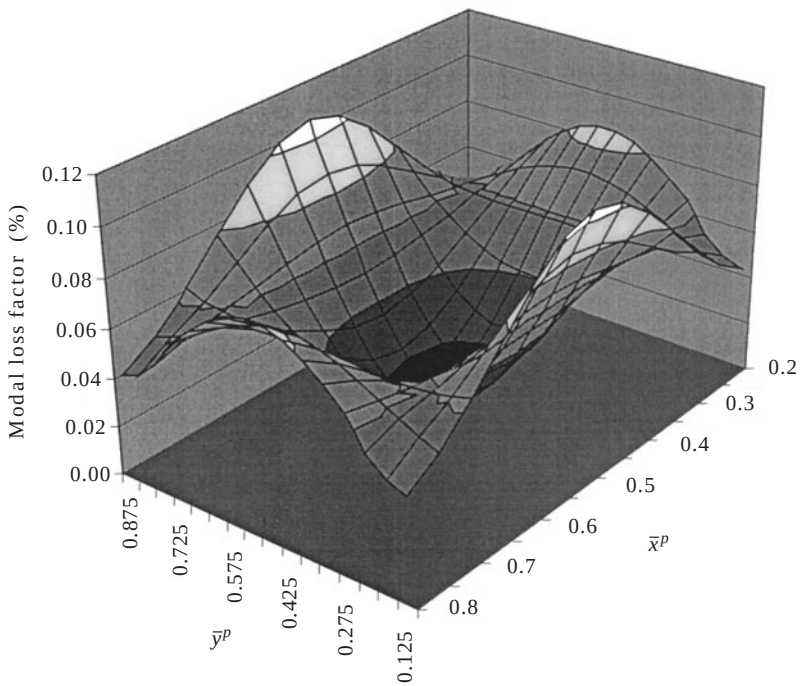

Figure 16. The 3-D loss factor map for mode (2, 1) of the rectangular plate of Table 6 and Figure 15 with free boundaries.

plate with free boundaries. The loss factor of mode (3, 3) is calculated using Method II when the patch width $\bar{l}_y^p$ is fixed at 0·2 and the axial length $\bar{l}_x^p$ is varying from 0 to 1. It is seen in Figure 14(a) that the loss factor increases with some fluctuations when $\bar{l}_x^p$ is increased. Similar results are seen in Figure 14(b) when $\bar{l}_x^p$ is fixed at 0·2 and $\bar{l}_y^p$ is varying from 0 to 1. Again, these fluctuations can be explained using the patch performance index $\mathscr{P}$ or the anti-node design concept.

The final parametric study is used to verify the patch performance index that suggests the best patch location(s). Once again consider the plate with free boundaries. Figure 15 shows the possible locations for a patch of size $\bar{l}_x^p = 0{\cdot}4$ and $\bar{l}_y^p = 0{\cdot}25$. Method II is again used to calculate the loss factor for mode (2, 1) over the region of possible patch locations. The 3-D loss factor map of Figure 16 shows that $(\bar{x}, \bar{y}) = (0{\cdot}5, 0{\cdot}125)$ and $(0{\cdot}5, 0{\cdot}875)$ are indeed the best locations for damping patch of the size mentioned above. But locations $(\bar{x}, \bar{y}) = (0{\cdot}2, 0{\cdot}5)$ and $(0{\cdot}8, 0{\cdot}5)$ may also be considered as candidates when four damping patches are to be applied. Similar studies may be carried out for other modes, using Methods II and III.

8. CONCLUSION

This paper has developed, examined, and validated three approximate methods for damping patch design studies. Given eigenfunctions of an undamped Euler beam, Method I avoids solving complex eigenvalue problems but still yields accurate results. Also, it is more than 50 times faster than the Rayleigh–Ritz methods [1] depending on the number of trial functions used. Method II further assumes a very compliant core and is computationally much faster than Method I. Method III is limited to a single compact patch application and the resulting patch index calculation is based on only one algebraic equation. Finally, Methods II and III are successfully extended to rectangular plates and the advantage in computational speed over the Rayleigh–Ritz method [2] is even more significant.

Based on the material presented in this article, the following design procedure is suggested.

(1) Select a particular mode of a beam or plate. Predict and plot patch performance indices using Method III over the entire surface. Place a damping patch at or near anti-nodes as a starting point. Choose a preliminary design concept including the number of patches and their locations in accordance with predictions.
(2) Using Method II for a plate and Method I or II for a beam, perform parametric design studies on the best possible locations for preliminary patches.
(3) Modify the design if necessary and perform parametric studies to achieve a desirable damping value for a given mode of interest.
(4) Apply these procedures for other modes of interest and determine the best design, using these methods iteratively, that provides the maximum possible damping over the frequency range of interest.
(5) Use the Rayleigh–Ritz method to confirm the final design concept. Validate the design by conducting modal or vibro-acoustic measurements.

The chief contribution of this article is the development of analytically simpler formulations that yield reasonable accurate results, in a computationally efficient manner, while providing much insight into the damping patch design concepts. Future work may include the development of an optimization scheme that considers several modes. Dynamic scaling issues for viscoelastically damped structures will also be addressed using the explicit form of the modal loss factor, as described by Method III.

ACKNOWLEDGMENT

This research has been supported by the Army Research Office (URI Grant DAAL 03-92-G-0120; 1992–97; Project monitor: Dr T. L. Doligalski). We thank the Wolverine Gasket Company for providing the damping material.

REFERENCES

1. S.-W. KUNG and R. SINGH 1998 *Journal of Sound and Vibration* **212**, 781–805. Vibration analysis of beams with multiple constrained layer damping patches.
2. S.-W. KUNG and R. SINGH 1998 *Journal of Sound and Vibration* **216**, 1–28. Complex eigensolutions of rectangular plates with damping patches.
3. A. D. NASHIF, D. I. G. JONES and J. P. HENDERSON 1985 *Vibration Damping*. New York: John Wiley & Sons.
4. C. T. SUN and Y. P. LU 1995 *Vibration Damping of Structural Elements*. Englewood Cliffs, NJ: Prentice Hall.
5. R. A. DITARANTO 1965 *Transactions of the American Society of Mechanical Engineers, Journal of Applied Mechanics* **87**, 881–886 Theory of vibratory bending for elastic and viscoelastic layered finite length beams.
6. M.-J. YAN and E. H. DOWELL 1972 *Transactions of the American Society of Mechanical Engineers, Journal of Applied Mechanics* **39**, 1041–1046. Governing equations for vibrating constrained-layer damping sandwich plates and beams.
7. D. J. MEAD 1982 *Journal of Sound and Vibration* **83**, 363–377. A comparison of some equations for the flexural vibration of damped sandwich beams.
8. A. K. LALL, N. T. ASNANI and B. C. NAKRA 1987 *Journal of Vibration, Acoustics, Stress, and Reliability in Design* **109**, 241–247. Vibration and damping analysis of rectangular plate with partially covered constrained viscoelastic layer.
9. A. K. LALL, N. T. ASNANI and B. C. NAKRA 1988 *Journal of Sound and Vibration* **123**, 247–259. Damping analysis of partially covered sandwich beams.
10. P. R. MANTENA, R. F. GIBSON and S. J. HWANG 1990 *AIAA Journal* **29**, 1678–1685. Optimal constrained viscoelastic tape lengths for maximizing damping in laminated composites.
11. J.-L. MARCELIN, P. TROMPETTE and A. SMATI 1992 *Finite Elements in Analysis and Design* **12**, 273–280. Optimal constrained layer damping with partial coverage.
12. T. ROOK 1995 *Ph.D. dissertation, The Ohio State University*. Vibratory power flow through joints and bearings with application to structural elements and gearboxes.
13. A. B. SPALDING and J. A. MANN III 1995 *Journal of the Acoustical Society of America* **97**, 3617–3624. Placing small constrained layer damping patches on a plate to attain global or local velocity changes.
14. D. S. NOKES and F. C. NELSON 1968 *Shock and Vibration Bulletin* **38**, Part 3, 5–10. Constrained layer damping with partial coverage.
15. D. J. GORMAN 1975 *Free Vibration Analysis of Beams and Shafts*. New York: John Wiley & Sons.

APPENDIX A: LIST OF SYMBOLS

a, b, c, d	coefficients
C	thickness parameter $(h_1 + 2h_2 + h_3)/2$
E	Young's modulus
e	elasticity ratio E_1h_1/E_3h_3
F	axial force
f	frequency (Hz)
$\mathscr{G}$	relative stiffness
G	shear modulus
$\mathscr{H}$	patch thickness index
h	thickness
I	area moment of inertia
$\mathscr{L}$	patch size parameter
l	length or width
N_p	total number of patches
N	total number of shape functions
$\mathscr{P}$	patch performance index
q	coefficient
r	trial eigenfunction number
s	spatial constant
T	kinetic energy
u	in-plane or longitudinal displacement
U	potential or strain energy
w	flexural displacement
x, y, z	spatial co-ordinates
Y	a stiffness and dimension parameter
ϕ	shape function
γ	shear deformation
η_k	modal loss factor of mode k
$\eta_{m,2}$	material loss factor of layer 2
η_p	modal loss factor contributed by patch p
λ	frequency parameter
μ	a constant related to stiffness, dimensions and frequency parameter
v	Poisson's ratio
ρ	mass density
τ	shear stress

Operators

d	differential operator

Superscripts

$\bar{}$	non-dimensionalized value
$\hat{}$	normalized quantity
p	patch number
k	modal index

Subscripts

a, b	patch ends
0	reference value for normalization
1	layer 1 (elastic constraining layer)
2	layer 2 (viscoelastic constrained layer)
3	layer 3 (base structure)
max	maximum
min	minimum

opt	optimum value
total	total value
u	in-plane motion
x, *y*	spatial co-ordinates
w	flexural motion
γ	shear deformation

APPENDIX B: DERIVATION OF THE SHEAR STRAIN TERM

Equation (4) may be derived by observing a segment of the deformed beam (Figure 2). Since rotation angles ($\psi^p_{xz,1}$ $\psi^p_{xz,2}$ and $\psi_{xz,3}$) are small, the longitudinal distance between the centers of layers 1 and 3 is given below in terms of rotations and layer thickness (h_1^p, h_2^p and h_3):

$$u_3 - u_1^p = \psi^p_{xz,1}\frac{h_1^p}{2} + \psi^p_{xz,2}h_2^p + \psi_{xz,3}\frac{h_3}{2}. \tag{B1}$$

Further, rotations of all layers are expressed in terms of the shear angles and the derivative of flexural displacement w with respect to $\bar{x}$; note that shear angles in layers 1 and 3 are ignored:

$$\psi^p_{xz,1} = \frac{\mathrm{d}w}{l_x\,\mathrm{d}\bar{x}}; \qquad \psi^p_{xz,2} = \frac{\mathrm{d}w}{l_x\,\mathrm{d}\bar{x}} - \gamma_2^p; \qquad \psi_{xz,3} = \frac{\mathrm{d}w}{l_x\,\mathrm{d}\bar{x}}. \tag{B2a–c}$$

Eliminating rotations by combining equations (B1) and (B2), the shear strain of layer 2 is obtained as

$$\gamma_2^p h_2^p = u_1^p - u_3 + \tfrac{1}{2}(h_1^p + 2h_2^p + h_3)\frac{\mathrm{d}w}{l_x\,\mathrm{d}\bar{x}}. \tag{B3}$$

Equation (B3) is the equation (4) of section 2.2.